Available online at www.sciencedirect.com

ScienceDirect

journal homepage: http://www.elsevier.com/locate/rpor

Original research article

Presenting and simulating an innovative model of liver phantom and applying two methods for dosimetry of it in neutron radiation therapy

Seyed Alireza Mousavi Shirazi, Ali Pazirandeh, Gholamreza Jahanfarnia, Mitra Athari Allaf*

Department of Nuclear Engineering, Science and Research Branch, Islamic Azad University, Tehran, Iran

ARTICLE INFO

Article history:
Received 11 April 2016
Received in revised form
26 June 2016
Accepted 29 September 2016
Available online 27 October 2016

Keywords:
Analytical approximation
Dose
Liver phantom
MCNPX code
Neutron
Radiation

ABSTRACT

Aim: A new model of liver phantom is defined, then this model is simulated by MCNPX code for dosimetry in neutron radiation therapy. Additionally, an analytical method is applied based on neutrons collisions and mathematical equations to estimate absorbed doses. Finally, the results obtained from two methods are compared to each other to justify the approach.

Background: The course of treatment by neutron radiation can be implemented to treat cancerous tissues, although this method has not yet been widespread.

The MIRD and the Stylized Family Phantom were the first anthropomorphic phantoms, although the representation of internal organs was quite crude in them. At present, a water phantom is usually used for clinical dosimetry.

Materials and methods: Each of the materials in an adult liver tissue including water and some organic compounds is decomposed into its constituent elements based on mass percentage and density of every element. Then, the accurate mass of every decomposed material of human liver tissue is correlated to masses of the phantom components.

Results: The absorbed doses are computed by MCNPX simulation and analytical method in all components and different layers of this phantom.

Conclusions: Within neutron energy range of 0.001 eV–15 MeV, the calculated doses by MCNPX code are approximately similar to results obtained by analytical method, and the derived graphs of both methods approve one another. It is also concluded that through increasing the incident neutron energy, water receives the largest amounts of absorbed doses, and carbon, nitrogen and sulfur receive correspondingly less amounts, respectively.

* *Corresponding author at*: Department of Nuclear Engineering, Science and Research Branch, Islamic Azad University, Hesarak Rd, Ashrafi Isfahani Hwy, Tehran, Iran.

E-mail addresses: a_moosavi@azad.ac.ir (S.A. Mousavi Shirazi), pzrud193y@srbiau.ac.ir (A. Pazirandeh).

http://dx.doi.org/10.1016/j.rpor.2016.09.013

Nomenclature

E_1	the energy of emitted neutron before collision
E_2	the energy of emitted neutron after collision
E_R	absorbed dose (transferred energy)
$\Sigma^H_{s(elastic)}$	macroscopic elastic scattering cross section for hydrogen
$\Sigma^C_{s(elastic)}$	macroscopic elastic scattering cross section for carbon
$\Sigma^C_{s_1(inelastic)}$	macroscopic nonelastic scattering cross section for the first excitation level of carbon
$\Sigma^C_{s_2(inelastic)}$	macroscopic nonelastic scattering cross section for the second excitation level of carbon
Σ_s	macroscopic scattering cross section
Σ^H_a	macroscopic absorption cross section for hydrogen
Σ^C_a	macroscopic absorption cross section for carbon
Σ_t	macroscopic total cross section
Ω	space angle
θ	collision angle of incident neutron
T	temperature
k	the Boltzmann constant
E_U	upper limit of integration for neutron energy
E_L	lower limit of integration for neutron energy

1. Background

Applying the neutrons is a new method in radiotherapy course for the treatment of cancerous tumors. First, the concept of neutron radiation therapy was shortly proposed after the discovery of the neutron by Chadwick in 1932.[1]

The neutron radiation therapy may be implemented in a patient through two types of neutrons. One type of neutron radiation therapy is Boron Neutron Capture Therapy (BNCT) that applies epithermal neutrons. It is considered that the available neutron beams in the epithermal-based reactors can mostly be an eligible source to produce epithermal neutrons to be applied in the BNCT. In the BNCT, the thermal reactors which provide low energy neutrons, might be used as a neutron source.[2]

Another type is Neutron Capture Therapy (NCT) that is relative to fast neutrons. In that case, it is suggested that the mono-energy neutrons be used. One choice is D-T source which produces 14 MeV neutrons. As Am-Be source produces a wide spectrum of neutron energies, it is not appropriate for this purpose.[3,4]

During radiotherapy by any radiation, it is always indispensable to stop the absorption of the excess dose by a normal tissue. On the other hand, measurement and assessment of absorbed dose is an important matter.[5] Thus, before practical treatment, a new phantom modeling might be very helpful for the sake of dose calculation. An appropriate software tool for this aim is the MCNPX code.[6]

One of the liver models which has already been applied in dosimetry is a small-scale dosimetry model for various source-target combinations within the micro-architecture of human liver and using Monte Carlo simulations. In this model, the ratio of local absorbed dose has been calculated to the whole-organ average absorbed dose.[7]

Another model is the simulation of a homeostatic liver lobule in which cell death, cell division, and changes in vasculature are all present. This model consists of a single classical hepatic lobule. The morphology and function of this lobule represents all lobules within the liver. In this model, a synthesized lobule is used for flow in histomorphometry data.[8]

At present, one of the most common phantom models is the "Water Phantom" that is used for clinical dosimetry. This phantom contains a water chamber such that a counter is placed at various points of it. In this phantom, the amount of transferred dose from existing water in tissue to tissue is calculated according to the following equation:

$$D_{tissue} = D_{water}\left(\frac{\tilde{\mu}_{en}}{\rho}\right) \quad (1)$$

In the "Dose Volume Histogram" (DVH) calculations, the phantom named "Test Phantom" is used in such a way that they have specified dimensions. These phantoms are mainly comprised of cubes and isocenter circles that are applied for testing the dose calculation accuracy.[9]

A crude model of phantom is MIRD phantom that has been developed in 1960 with 22 internal organs and more than 100 sub-regions. It is the first anthropomorphic phantom representing a hermaphrodite adult for internal dosimetry. The major type of phantom named "Stylized Family Phantom" series were also developed, although the representation of internal organs was quite crude in these phantoms, as it had many inherent limitations in definition of geometry and material of each organ.[10]

The liver is the second largest single organ in the body (after the skin), weighing on average 2 kg in an average adult. In actual state, the average width of the liver tissue across for an adult human is approximately 21–22.5 cm, the vertical height of this organ at the greatest height is estimated to be 15–17.5 cm, and the depth is 10–12.5 cm from the front to back.[11] The liver tissue is located in the right upper quadrant of the abdominal cavity, resting just below the diaphragm. The liver lies to the right of the stomach, and its left lobe is accessible for radiation, although, the liver is wider.[12]

2. Aim

There are three prime objectives of this investigation:

a) The first objective is to define a new model of a liver phantom and simulation of it by the MCNPX code. This phantom has identical compositions compared with existing compositions in a human liver tissue; so, in this study, each of the materials in an adult liver tissue (including water, protein, glucose and glycogen) is decomposed to its constituent elements. This decomposition is carried out based on the mass percentage and density of every element, then the accurate mass of every analyzed element (such as H, O, C, N and S), which exists in constituent materials of the

liver tissue, is associated with the mass of components of the mentioned phantom.[13]

b) The second objective is to introduce an analytical method to calculate absorbed doses using mathematical equations and computer programming, and then comparison between the results obtained from the analytical method and MCNPX code to survey validation of this method.[14]

c) The third objective is to study the interaction of neutrons in a real liver tissue and also the consideration of incident neutron energy emitted from clinical neutron source for a wide range of neutrons in neutron capture therapy.

3. Materials and methods

In this research, a spherical model of liver phantom is defined, then it is simulated by the MCNPX code. This phantom might also have variable radii. It means that it might be bigger or smaller than applied dimensions in this investigation, and might really be equivalent to dimensions of livers belonging to either minor or major. In this study, this phantom has been taken from an average weight of a real liver tissue, i.e. 2 kg. But if the weight of the liver tissue is bigger or smaller than this mean value, the thickness and radius of each sphere will be changed correspondingly.

Despite the fact that the spherical shape of a phantom is different from a real liver tissue geometry, in this research the spherical liver model has been applied. The reasons being:

Firstly, in this research, the main aim is to invent a simple way to study the neutron behavior and neutron interaction in a virtual liver tissue for dosimetry using both the MCNPX code and the analytical method.
Secondly, determining the precise volume of a real liver tissue with the aim of calculating phantom dimensions is very difficult as the shape of the liver tissue is not uniform. In so doing, a symmetric spherical-shape phantom is considered.
Thirdly, the different shapes of a phantom, like a cubic shape, have already been applied by scientists as body limb in some studies.

However, generally, in such kind of research phantom, the main objective is to simulate the nuclear interactions in the material.[15,16]

The laboratory experiments have already rendered the precise molecular composition of the liver tissue according to Table 1.[17]

The constituent compounds of human liver tissue, which have been detailed in Table 1, compose the liver tissue and are distributed across it. These compounds have been extracted from chemical decomposition of a real liver tissue.

Table 1 – The components and structural materials of a real liver tissue.

Mass percentage	Material
69.69%	Water
0.35%	Glycogen ($C_{24}H_{42}O_{21}$)
29.90%	Protein and glucose ($C_{44189}H_{71252}N_{12428}O_{14007}S_{321}$ and $C_6H_{12}O_6$)

Due to the shape of liver tissue not being uniform and difficulty in defining geometry in it, defining a symmetric phantom is very important. Therefore, since the main aim is to turn the real liver tissue into a mathematical model for the sake of dosimetry in neutron therapy, a spherical model of phantom is considered because of its symmetry in such a way that it consists of materials analogous to the existing compounds in a real liver, and each layer meets the related dimension, and is filled up with the related material.[18]

The advantage of the proposed spherical model is that it is a simple flexible model created from a liver tissue for the purpose of dose calculation consisting of all constituent materials in a real liver tissue, and the neutron beam path has been accurately considered in it.

This phantom has two main parts. The first part is the spherical layers, and the second part is the cylindrical neutron beam path.

After analyzing the structural components of liver tissue (weighing 2 kg) based on their mass percentage and densities into their constituent elements consisting of H, O, C, S and N, the amounts of H and O are incorporated into the water and the amounts of other elements including C, S and N are accordingly calculated as accurately as possible. Thus, the masses of every analyzed element and also the thicknesses and radii of hypothetical spheres are obtained as shown in Table 2.

This phantom is comprised of a water sphere in such a way that its radius is considered to be 2.737 cm. This water sphere is surrounded with a layer of carbon according to Table 2, the hypothetical outside radius and thickness of the mentioned layer are 3.437 cm and 7 mm, respectively. There is an outside thin layer of sulfur with the thickness of 197.2 μm that covers around the carbon layer. This set is entirely encased in a spherical shell of carbon as a reflector with the inside radius and thickness of 27.00 cm and 3 mm, respectively. This layer acts as a reflector to decrease the escaping of the fast neutrons. The blank space between the sulfur layer and the carbon shell

Table 2 – Mass, outside radius and thickness belonging to every analyzed element.

Elements	Mass (g)	Outside radius of related sphere (cm)	Thickness (cm)
C	316.93	3.437 (inner carbon shell) 27.34 (outer carbon shell)	0.7 0.33
S	6.08	3.456	0.019
N	102.94	27.004	23.547
H	198.9	Incorporated into the water sphere with radius: 2.737 cm	
O	1373.93		

Table 3 – The compositions of adipose tissue of males.

Percentage of standard weight	Number	Water (g/100 g)	Fat (g/100 g)	Protein (g/100 g)
70–79	4	14.4	83.5	3.2
80–89	13	17.9	78.2	3.3
90–99	15	13.5	82.8	2.6
100–109	9	10.2	87.2	2.1
110–119	12	10.3	87.2	2.7
120–160	8	9.6	88.2	2

is filled up with nitrogen gas. This blank space has inside and outside radii of 3.456 cm and 27.004 cm, respectively.

To better design this phantom, a hypothetical narrow neutron beam path is also accurately considered as a cylindrical path within the skin and adipose tissues which is in front of the liver tissue with the neutron passing through it to reach the liver tissue. Of course, as the point neutron source is located on the nearest section of the patient body in neutron capture therapy, this distance is very short. This distance has a cylindrical shape, and plays the role of a collimator. One of the most important tissues, which lies in front of the liver, is adipose tissue.

Table 3 shows the existing compositions in adipose tissue of males.

The adipose tissue is comprised of water, fat and protein.[19] Water and fat make up together typically more than 90% of the body adipose tissue mass.[20] The adipose tissues have varied thicknesses (0–10 mm, 11–20 mm, 21–30 mm, 31–40 mm) in different individuals. It depends on age and on whether a person is fat or slim. In this investigation, the thickness of adipose tissue, which has been considered for the simulation, is 30 mm.[21] One of the components of adipose tissue is fat. The chemical formula of fat is: CH2ORCHOR′CH2OR. Fat is not actually a compound. It is a mixture of many esterified acids named: fatty acids. In connection with skin tissue, the average skin thickness is thicker in males than females. A pure average skin thickness is 1.5 mm in males. The skin and the subcutaneous tissue consist of some portions such as epidermis, dermis, hypodermis and fat. Skin is not a single substance, so it does not have a single formula. It is made mostly of various proteins, water, fat and salt. Skin is a biological tissue which consists of carbon, oxygen and nitrogen.[22]

The average distance between body surface (nearest section into the body for setting the neutron source collimator) and liver tissue is considered to be 3 cm for a normal body. Additionally, the diameter of neutron source head is considered to be 3 cm. Thus, after decomposing both the adipose and skin compounds into their components, given the masses and volumes of each of the compounds, the inside and outside radii of the neutron path are calculated as accurately as possible. The mass value of each existing component in this cylindrical path and the path radii are shown in Table 4.

Table 4 – The mass amount of each component and neutron path radii.

Compositions	Mass	Radii (cm)
Water	1.95	Incorporated into a cylindrical
Fat	16.72	path with inside and outside radii:
Protein	0.4	1.5 cm and 2.1 cm, respectively

The side view of the liver lying in abdominal tissue besides the cylindrical neutron path that have been converted into the liver phantom in section (a) and the schematic view of the liver phantom in section (b) have been illustrated in Fig. 1, respectively.

In the present work, neutrons are supposed to be emitted from an external source, and after passing through the layers of phantom and lots of collision with other nuclei and consequently slowing down, the deposited energy in the materials of phantom are computed by both the MCNPX code and the analytical method.

3.1. *Simulation of phantom by MCNPX code*

Fig. 2 shows the simulated view of the phantom that has been simulated by the MCNPX code.

The applied tally in this research is F6. The F6 is applied for estimation of energy deposition. For a well-behaved tally, relative error (R) will be proportional to $1/\sqrt{N}$, where N is the number of histories. The specification of tallies (F*n*) is carried out according to Table 5.

Both compositions and geometrical data belonging to liver phantom have been inputted into the MCNPX code. In this simulation, the mentioned neutron path has been accurately taken into consideration.

3.2. *Analytical method*

In this stage, to improve the performance, another method is introduced by analytical method for estimating the absorbed doses instead of the transport equation that MCNP code uses.

It is necessary that both neutron scattering cross section and its angular distribution (due to neutron penetration in the liver phantom) be obtained. When a neutron moves through the matter, there are three major types of interactions with nuclei. These are elastic scattering, nonelastic scattering, and absorption. Collision of neutron on carbon and hydrogen nuclei causes an amount of energy to be transferred from neutron to the target nucleus. The recoiled nucleus moves a short distance through the matter and deposits its energy along the path. In this case, the main problem is to compute the energy

Table 5 – Tally specification cards.

F1:P	F1:E	Surface current
F2:P	F2:E	Surface flux
F4:P	F4:E	Track length estimate of cell flux
F5:P		Flux at a point (point detector)
F6:P		Track length estimate of energy deposition
F8:P	F8:E	Energy distribution of pulsed created in a detector

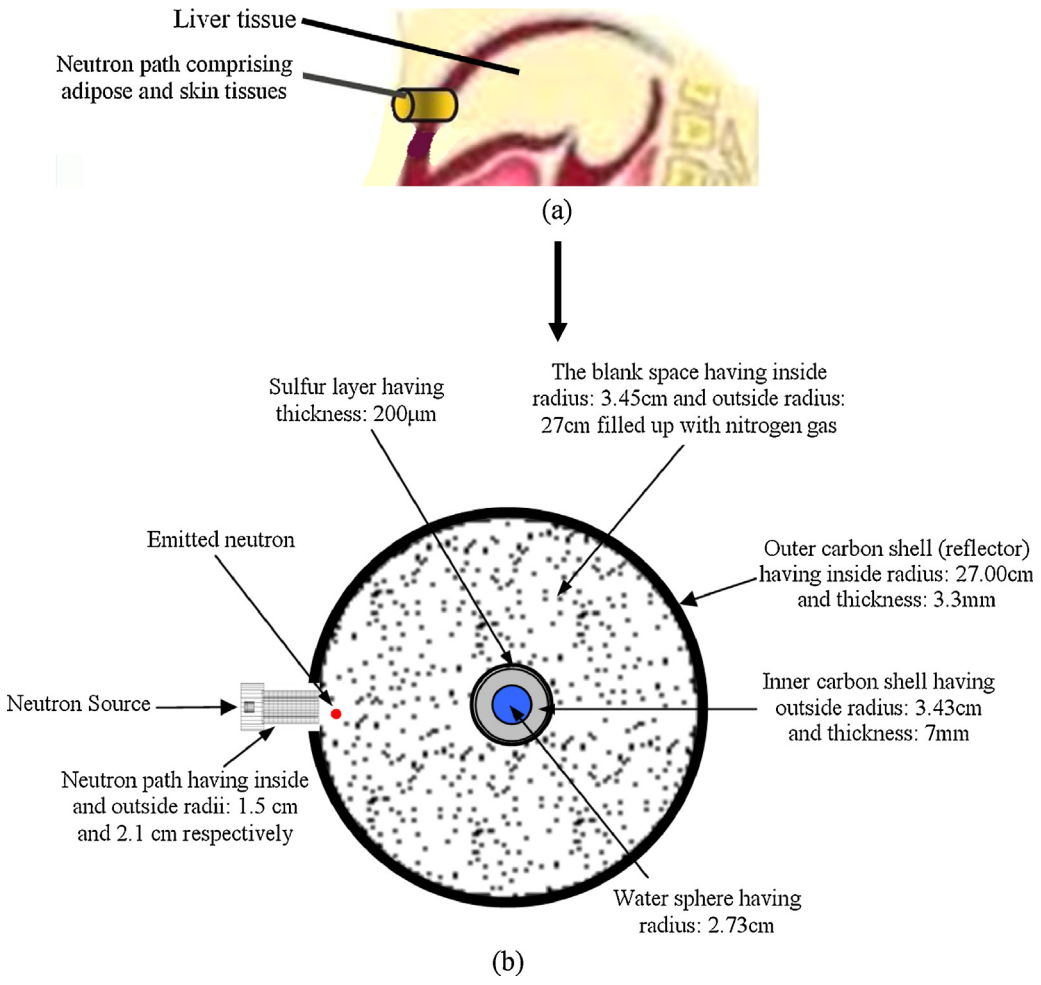

Fig. 1 – (a) The side view of the neutron path and liver tissue. (b) The schematic view of the liver phantom.

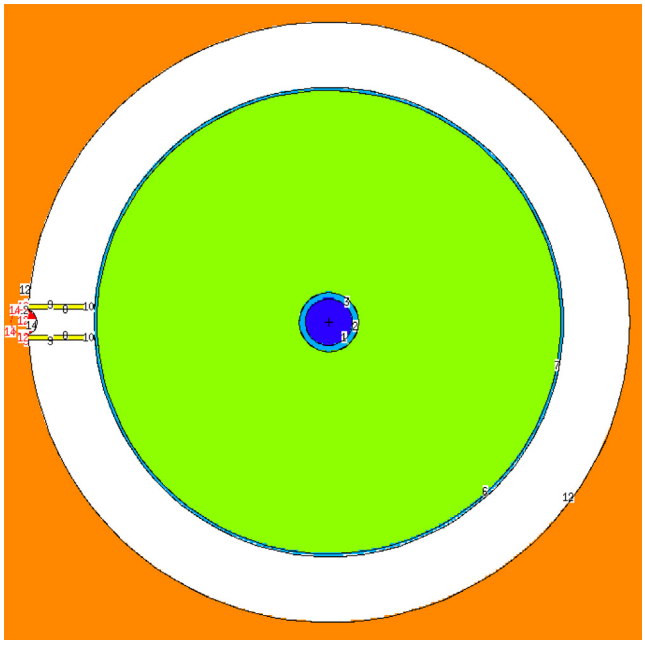

Fig. 2 – The phantom simulated by the MCNPX code.

of recoiled nucleus. In order to apply the analytical method, the collision history of each neutron might be tracked in which it either is absorbed or scattered in the volume of material.[23]

The nonelastic scattering of neutron in carbon is also important to be considered. Thus, a significant value of energy is absorbed in the recoiled nucleus and E_R is less than the energy of scattered neutrons.[24]

Each of the neutron collision events (e_1, e_2, …, e_n) is associated with the related probability (P_1, P_2, …, P_n). All the events, which are shown through e_i, are held up as a neutron reaction with target nuclei. By selecting a random number (R), every event is sampled, if:

$$\left(\sum_{i=1}^{j-1} P_i\right) \leq R \leq \left(\sum_{i=1}^{j} P_i\right) \tag{2}$$

where:

$$\sum_{i=1}^{n} P_i = 1 \tag{3}$$

In the process of neutron transport in liver phantom, it is subject to three major types of interactions with carbon,

hydrogen, nitrogen and sulfur nuclei. The major interactions are elastic scattering, nonelastic scattering, and absorption. Each type of interaction correlates with a specific probability having a relative proportion to the interaction cross section according to the following equations (Eqs. (4)–(10)):

$$P_1 = \frac{\sum_{s(elastic)}^{H}}{\sum_s} \tag{4}$$

$$P_2 = \frac{\sum_{s(elastic)}^{C}}{\sum_s} \tag{5}$$

The probability of nonelastic scattering in carbon (for the first excitation level in 4.43 MeV):

$$P_3 = \frac{\sum_{s_1(nonelastic)}^{C}}{\sum_s} \tag{6}$$

The probability of nonelastic scattering in carbon (for the second excitation level in 7.65 MeV):

$$P_4 = \frac{\left[\sum_{s_2(nonelastic)}^{C}\right]}{\sum_s} \tag{7}$$

The probability of scattering in nitrogen:

$$P_5 = \frac{\sum_{s(elastic)}^{N}}{\sum_s} \tag{8}$$

The probability of scattering in sulfur:

$$P_6 = \frac{\sum_{s(elastic)}^{S}}{\sum_s} \tag{9}$$

The probability of neutrons absorption in hydrogen, carbon, nitrogen and sulfur:

$$P_7 = \frac{\left[\sum_a^H + \sum_a^C + \sum_a^N + \sum_a^S\right]}{\sum_t} \tag{10}$$

If all the directions in angle distribution are the same, the scattering will be isotropic. The fraction of emitted neutrons for isotropic state is as follows:

$$P(\Omega)d\Omega = \frac{d\Omega}{4\pi} = \frac{2\pi d(\cos\theta)}{4\pi} = \frac{1}{2}d(\cos\theta) \tag{11}$$

The absorbed dose or, on the other hand, the lost energy of neutron in each scattering is described by Eq. (12) [25]:

$$E_R = \Delta E = E_1 - E_2 = (\cos\theta)P(\cos\theta)d(\cos\theta) \tag{12}$$

where the probability of $P(\cos\theta)d(\cos\theta)$ is obtained in the θ to $\theta + \Delta\theta$ range by Eq. (13):

$$P(\cos\theta)d(\cos\theta) = \frac{1}{2}[\cos\theta - \cos(\theta + \Delta\theta)] \tag{13}$$

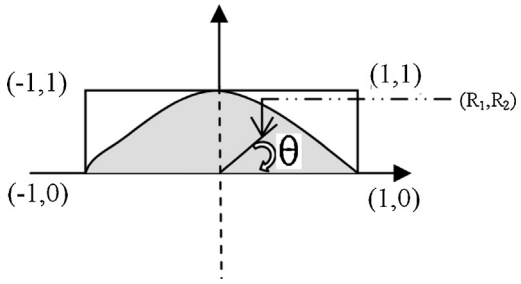

Fig. 3 – The semicircle encased at a rectangle to generate random numbers.

and:

$$\overline{\cos\theta} = \int_{-1}^{+1} \cos\theta P(\cos\theta)d(\cos\theta) \tag{14}$$

Random sampling technique can help compute $\cos\theta$ for $0 < \theta < 2\pi$. These random numbers are generated at a semicircle encased at a rectangle which has four vertexes in $(-1, 0)$, $(-1, 1)$, $(1, 1)$ and $(1, 0)$ according to Fig. 3.

In turn, two random numbers named R_1 and R_2 are generated since Eq. (15) is set as follows:

$$\cos\theta = \frac{R_1}{\sqrt{R_1^2 + R_2^2}} \tag{15}$$

On the condition that: $-1 \le R_1 \le +1$ and $0 \le R_2 \le +1$. If: $(R_1^2 + R_2^2) > 1$, then this pair of random numbers is discarded, and new random numbers are selected, and this procedure is repeated over and over again. The scattering between neutron and hydrogen nucleus is isotropic for the energies below 14 MeV. As the atomic weights of carbon, nitrogen and oxygen are grater than other nuclei, the scattering angle is approximately the same in either laboratory or the center of mass systems. So, this angle is within the range of $[0, 2\pi]$.

Since a significant percentage of the liver is made up of hydrogen, the interaction of neutron with hydrogen must be studied as accurately as possible. Approximately 85–95% of neutron energy transferred to the liver tissue is attributed to its interaction with hydrogen. For high energies, (n, α) reactions play a very significant role among all the reactions, and make the considerable fraction of absorbed dose in the tissue. In this state, some part of absorbed dose is because of α particles.

In nonelastic reactions, the angular distribution of both incident neutron and the recoiled nucleus become more complicated than lower energies. In high energies, the contribution of recoiled proton (hydrogen nucleus) causes more than 60% of energy deposition, and the rest of deposited energy is because of α particle in addition to other heavy nuclei.[26] Therefore, computation of transferred energy is held up as a very important matter in nonelastic scattering.

Studying the penetration of neutron in a liver phantom and its interaction in water is subject to precise knowledge about interaction cross sections and angular distribution of the scattered neutron.[25] For this purpose, the microscopic cross sections of absorption and scattering for H, C, N and

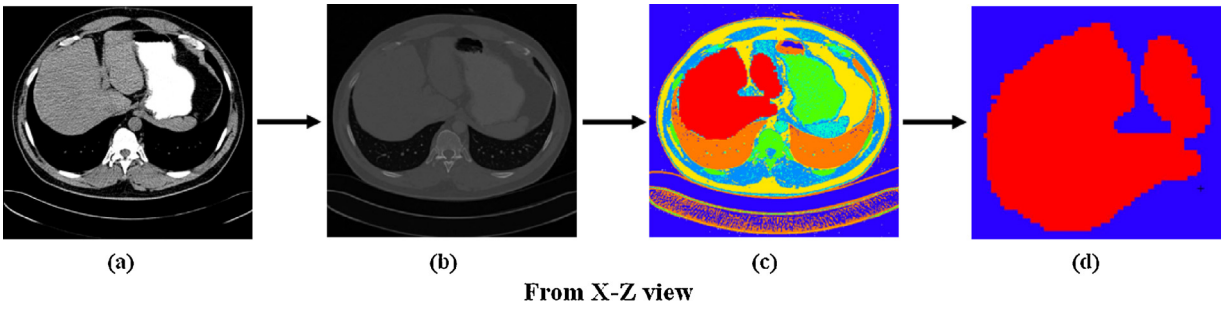

Fig. 4 – (a) The image of abdominal tissue slice using CT scanning. (b) The image of abdominal tissue converted by a specific MATLAB software. (c) The image of abdominal tissue converted by the MCNPX code from MATLAB software. (d) The image of segmented liver tissue shown by the MCNPX code.

S are extracted from programming by the MCNPX code based on defining the mentioned elements, and then this data is applied to calculate all the probabilities for a wide range of neutron energies, although there might be another way to obtain the mentioned data. This way is that the initial microscopic cross sections of absorption and scattering are used from the library of JENDL-3.2 at 300 K for the mentioned elements, and this data is computed by Eqs. (16)–(18) for multi-group neutrons; thereby, the new microscopic cross sections of absorption and scattering may both be obtained within the energy interval of each of the neutron groups. The equation which can be applied for Maxwellian spectrum is according to Eq. (16)[27,28]:

$$\sigma_{macs}(T) = \frac{2}{\sqrt{\pi}} \frac{\int_{E_L}^{E_U} \sigma(E,T)\cdot E\cdot \exp\left(\frac{-E}{kT}\right) dE}{\int_{E_L}^{E_U} E\cdot \exp\left(\frac{-E}{kT}\right) dE} \quad (16)$$

For resonance spectrum:

$$\sigma_{res}(T) = \int_{E_L}^{E_U} \sigma(E,T)\cdot \frac{1}{E} dE \quad (17)$$

Additionally, Eq. (18) is used for fission spectrum as below:

$$\sigma_{fis} = \frac{\int_{E_L}^{E_U} \sigma(E,T)\cdot \sqrt{\frac{4}{\pi a^3 b}}\cdot \exp\left(-\frac{ab}{4}-\frac{E}{a}\right)\cdot \sinh\sqrt{bE}\, dE}{\int_{E_L}^{E_U} \sqrt{\frac{4}{\pi a^3 b}}\cdot \exp\left(-\frac{ab}{4}-\frac{E}{a}\right)\cdot \sinh\sqrt{bE}\, dE} \quad (18)$$

where a and b are 0.988 and 2.249, respectively.

In turn, using Turbo Pascal or FORTRAN programming and considering incident neutron energy as E_1 as input data to the program in the neutron energy range of 0.001 eV–17 MeV, the absorbed doses in all components of the liver phantom are computed in Gray.[29] The computer programming which has

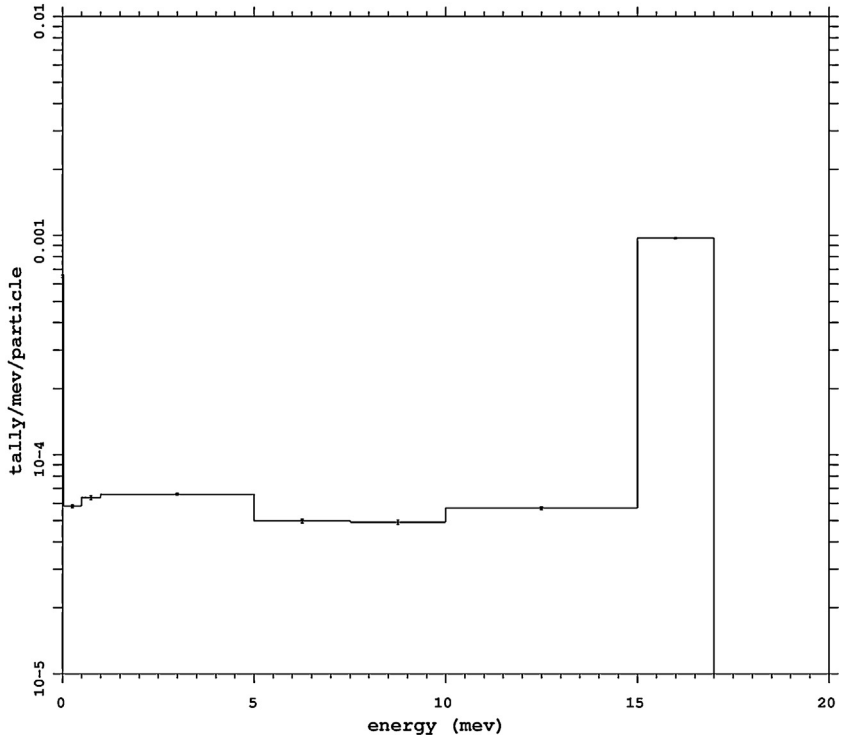

Fig. 5 – The total absorbed dose in the liver phantom obtained by MCNPX simulation (plotted by MCNPX code).

been developed in the present work computes the transferred energy from incident neutrons into the liver phantom based upon a proper approximation.[30]

3.3. *Experimental verification of the phantom model*

To better verify the phantom model experimentally, this matter is clinically considered and developed in this research.

The absorbed dose in a real liver tissue is calculated, and its result is compared with the result of a prepared liver model. The CT scan Di.Com images of a male with normal liver tissue are provided. Using specific MATLAB software called CT to MCNP, an abdominal tissue is simulated, and the liver tissue is wholly separated, and the accurate absorbed dose is obtained in it. In this software, the type of each of the existing materials in the abdominal tissue is recognized based on the level of Haunsfield unit (HU). By this method, every liver tissue can be simulated by self-CT images. Some of the images (belonging to one slice of Di.Com images) are consecutively illustrated in four stages in Fig. 4.

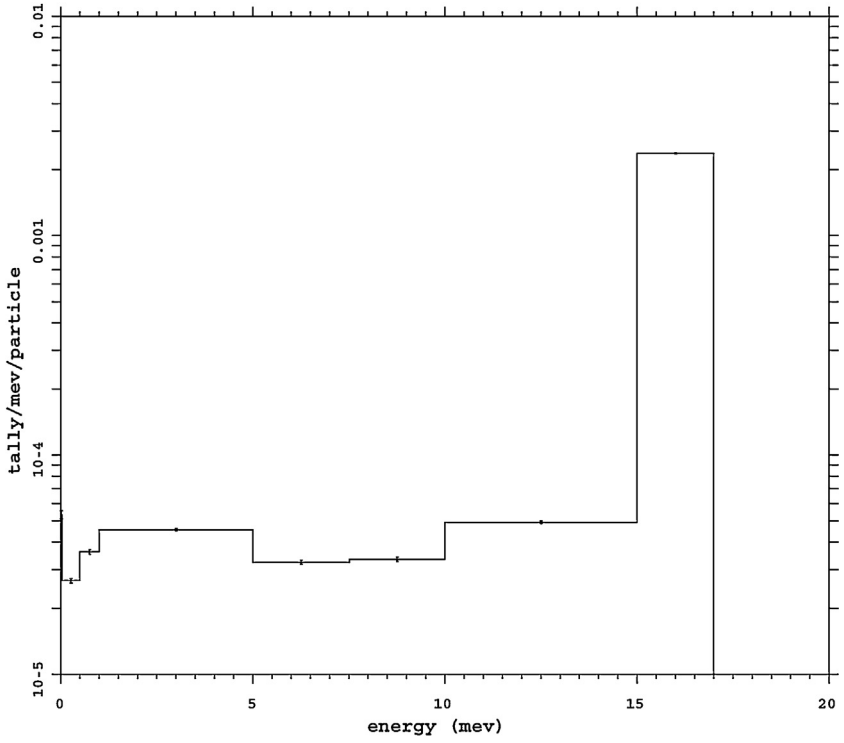

Fig. 6 – The total absorbed dose in the separated liver tissue (plotted by the MCNPX code).

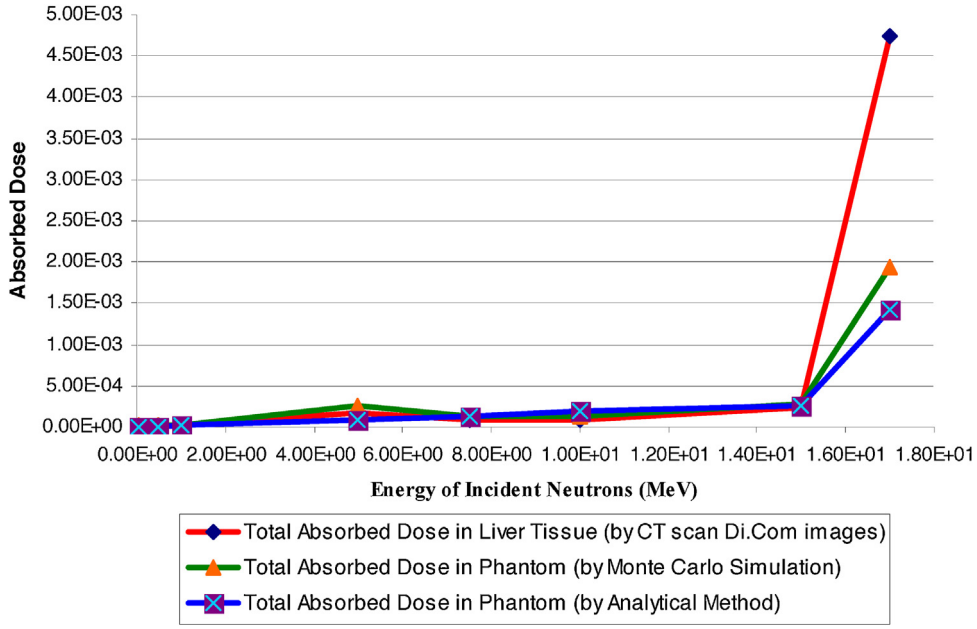

Fig. 7 – The total absorbed dose in the phantom obtained by both MCNPX simulation and analytical method.

4. Results

The derived graphs for absorbed dose in $E_1 - E_R$ by both MCNPX simulation and analytical method are shown in Figs. 5–7.

By this simulation, every human liver tissue can be changed into its associated phantom, and the amount of absorbed dose for neutron capture therapy of each of real liver tissues, which have various dimensions and sizes, might be studied. It means that for the sake of clinical aspect, this simulation might also be carried out in actual state for various forms and sizes of the liver. Of course, this modeling might be utilized for every tissue of body parts in which the related tissue has been decomposed to its constituent compounds and elements.

5. Conclusions

This modeling can be extended to other liver tissues. The comparison between the amount of absorbed doses obtained from the prepared liver model and the real liver tissue implies that the absorbed dose by the two methods agree with each other for neutron energies below 15 MeV. This suggests that this phantom can be applied for dosimetry and for the sake of studying neutron behavior in material.

In this study, the results obtained from the two methods are compared with each other. The absorbed energy due to thermal and epithermal neutron irradiation in each of the phantom components is insignificant and of little relevance.

According to Fig. 7, it is observed that within the neutron energy range of 0.001 eV–15 MeV, the calculated doses by analytical method are approximately similar to the results obtained by the MCNPX code and the derived graphs of both methods match each other for neutron energy below 15 MeV. For neutron energy above 15 MeV, the results of these two methods show a significant error. This is because the MCNPX code carries out all the dose calculations based on neutron tracking and transport equation, while the analytical method provides dose calculation based upon mathematical equations.

Therefore, due to the restriction of analytical method and its inability to include the α particles and consequently to compute computing the absorbed dose resulting from α particles, there is a disparity between the illustrated figures of MCNPX code and analytical method. Of course, it may not be an important problem, because the eligible range of neutrons for neutron capture therapy is within the range of neutrons where their absorbed doses agree in the figures of both methods.

Conflict of interest

None declared.

Financial disclosure

None declared.

REFERENCES

1. *Current status of neutron therapy*. Vienna, Austria: International Atomic Energy Agency; 2001, May. IAEA-TECDOC-1223.
2. Postuma I, Bortolussi S, Protti N, et al. An improved neutron autoradiography set-up for ^{10}B concentration measurements in biological samples. *Rep Pract Oncol Radiother* 2016;**21**:123–8.
3. Koivunoro H, Bleuel D, Nastasi U, et al. BNCT dose distribution in liver with epithermal D–D and D–T fusion-based neutron beams. *Appl Radiat Isot* 2004;**61**:853–9.
4. Khosroabadi M, Farhood B, Ghorbani M, et al. Tissue composition effect on dose distribution in neutron brachytherapy/neutron capture therapy. *Rep Pract Oncol Radiother* 2016;**21**:8–16.
5. Emiliano C, Pozzi C, Thorp S, et al. Intercalibration of physical neutron dosimetry for the RA-3 and MURR thermal neutron sources for BNCT small-animal research. *Appl Radiat Isot* 2011;**69**:1921–3.
6. Tagami T, Nishimura S. Intercalibration of thermal neutron dosimeter glasses NBS-SRM612 and corning 1 in some irradiation facilities: a comparison. *Int J Radiat Appl Instrum D* 1989;**16**:11–4.
7. Stenvall A, Larsson E, Strand SE, Jönsson BA. A small-scale anatomical dosimetry model of the liver. *Phys Med Biol* 2014;**59**:3353–71.
8. Wambaugh J, Shah I. A model for micro-dosimetry in virtual liver tissues. In: *The 10th international conference on systems biology*. 2009.
9. Kramer R, Cassola VF, Khoury HJ, et al. FASH and MASH: female and male adult human phantoms based on polygon mesh surfaces: II. Dosimetric calculations. *Phys Med Biol* 2010;**55**:163–89.
10. Fisher HL, Snyder WS. *Variation of dose delivered by 137Cs as a function of body size from infancy to adulthood*. Oak Ridge National Laboratory (ORNL); 1966.
11. Mousavi Shirazi SA, Sardari D. Design and simulation of a new model for treatment by NCT. *Sci Technol Nucl Install* 2012;**2012**:1–7, http://dx.doi.org/10.1155/2012/213640.
12. Kumar V, Abbas AK, Fausto N, Robbins SL, Cotran RS. *Robbins and Cotran pathologic basis of disease*. Liver and Gallbladder, USA: Elsevier Saunders; 2005. p. 821–81.
13. Daiki S, Kaoru S, Fumiaki T, Akira E. Monte Carlo simulation using Japanese voxel phantoms to analyze the contribution of particle types and their energy distributions to organ doses upon external neutron exposure. *J Nucl Sci Technol* 2010;**47**:62–9.
14. Zhang H, Liu Q, Qin B, Bo H. Simulating particle collision process based on Monte Carlo method. *J Nucl Sci Technol* 2015;**52**:1393–401.
15. Dhairyawan M, Nagarajan P, Venkataraman G. Response functions of spherically moderated neutron detectors. *Nucl Instrum Methods* 1980;**169**:115–20.
16. Reginatto M. What can we learn about the spectrum of high-energy stray neutron fields from Bonner sphere measurements. *Radiat Meas* 2009;**44**:692–9.
17. McBride J, Mason M, Scott E. The storage of the major liver components. *Biol Chem* 1941;**1**:943–52.
18. Herranz Crespo R, Domene MM, Prieto Rodríguez MJ. Biodosimetry and assessment of radiation dose. *Rep Pract Oncol Radiother* 2011;**16**:131–7.
19. Lorette WT. The chemical composition of adipose tissue of man and mice. *Exp Physiol* 1962;**47**:179–88.
20. Martin AD, Daniel MZ, Drinkwater DT, Clarys JP. Adipose tissue density, estimated adipose lipid fraction and whole body adiposity in male cadavers. *Int J Obes Relat Metab Disord* 1994;**18**:79–83.

21. Otte JW, Merrick MA, Ingersoll CD, Cordova ML. Subcutaneous adipose tissue thickness alters cooling time during cryotherapy. *Arch Phys Med Rehabil* 2002;**83**: 1501–5.
22. Broder V. Observations on skin thickness and subcutaneous tissue in man. *Z Morphol Anthropol* 1960;**50**:386–95.
23. Vega H, Hernández V, Manzanares E, et al. Neutron spectrometry using artificial neural networks. *Radiat Meas* 2006;**41**:425–31.
24. Chuncheng J, Kegel G, Egan J, et al. Measurement of U-235 fission neutron spectra using a multiple gamma coincidence technique. In: *International conference on nuclear data for science and technology, AIP conf*. 2004.
25. Mousavi Shirazi SA, Taheri A. A new method for neutron therapy (neutron therapy) and related simulation by MCNP4C code. In: *International conference on neutron and X-ray scattering in advancing materials research, AIP conf*. 2009.
26. Li T, Fang D, Li H. A Monte Carlo design of a neutron dose-equivalent survey meter based on a set of ^{3}He proportional counters. *Radiat Meas* 2007;**42**:49–54.
27. Tsuneo N, Keiichi S, Satoshi C, et al. Japanese evaluated nuclear data library, version 3 revision-2; JENDL-3.2. *J Nucl Sci Technol* 1995;**32**:1259–71.
28. Keiichi S, Tsuneo N, Hidemitsu S, Hiromitsu K. *Curves and tables of neutron cross sections in JENDL-3.2. JAERI-Data/Code 97-003*; 1997.
29. Mousavi Shirazi SA. Numerical solution of diffusion equation to study fast neutrons flux distribution for variant radii of nuclear fuel pin and moderator regions. *Kerntechnik* 2015;**80**:291–4.
30. Rafiei Karahroudi M, Mousavi Shirazi SA. Study of power distribution in the CZP, HFP and normal operation states of VVER-1000 (Bushehr) nuclear reactor core by coupling nuclear codes. *Ann Nucl Energy* 2015;**75**:38–43.